

AER1216H: Fundamentals of UAS Project (2023F)

Final Project Report

Group 10

Pouya Asgharzadeh – 1*****389

Vic Gao – 1*****613

Min Woo Kong – 1*****435

December 17, 2023

Table of Contents

OVERVIEW.....	1
FIXED-WING.....	2
DESIGN OBJECTIVE.....	2
AIRCRAFT DYNAMICS.....	2
AUTOPILOT DESIGN	2
TRIM CONDITION.....	4
VELOCITY CONTROL.....	5
ALTITUDE CONTROL	5
COORDINATED TURN CONTROL	6
SIDESLIP CONTROL	6
PERFORMANCE.....	7
<i>Windless Case</i>	7
<i>Wind Case</i>	9
THEORETICAL RESULT VS SIMULATION.....	11
<i>Angle of Attack</i>	11
<i>Yaw Rate</i>	11
<i>Climb Rate</i>	11
RANGE AND ENDURANCE CALCULATIONS.....	13
<i>Endurance</i>	13
<i>Range</i>	13
MULTI-ROTOR	15
DESIGN OBJECTIVE.....	15
MULTI-ROTOR DYNAMICS.....	15
CONTROL DESIGN	16
PERFORMANCE.....	18
RANGE AND ENDURANCE.....	21
CONCLUSIONS AND LESSONS LEARNED	22
REFERENCES	24

List of Tables

TABLE 1 - SUMMARY OF SIMULATION VS THEORETICAL RESULTS	12
TABLE 2 - STATE-SPACE INPUTS AND OUTPUTS USED FOR DYNAMICS MODEL.....	15

List of Figures

FIGURE 1 - FIXED-WING OVERALL SYSTEM DESIGN	3
FIGURE 2 - FIXED-WING STATE ESTIMATOR SYSTEM.....	4
FIGURE 3 - FIXED-WING CONTROL SYSTEM - VELOCITY CONTROL	5
FIGURE 4 - FIXED-WING CONTROL SYSTEM - ALTITUDE CONTROL.....	5
FIGURE 5 - FIXED-WING CONTROL SYSTEM - COURSE RATE CONTROL.....	6
FIGURE 6 - FIXED-WING CONTROL SYSTEM - SIDESLIP CONTROL.....	6
FIGURE 7 - FIXED-WING 3D POSITION PLOT AS TIME CHANGES UNDER WINDLESS CONDITION - 3D VIEW (TOP) & X-Y VIEW (BOTTOM).....	7
FIGURE 8 - FIXED-WING SIMULATION RESULTS UNDER WINDLESS CONDITION	8
FIGURE 9 - FIXED-WING DE, DA, DR, AND DT RESULTS UNDER WINDLESS CONDITION	8
FIGURE 10 - FIXED-WING 3D POSITION PLOT AS TIME CHANGES UNDER WIND CONDITION - 3D VIEW (TOP) & X-Y VIEW (BOTTOM).....	9
FIGURE 11 - FIXED-WING SIMULATION RESULTS UNDER WIND CONDITION	10
FIGURE 12 - FIXED-WING DE, DA, DR, AND DT RESULTS UNDER WIND CONDITION	10
FIGURE 13 - FIXED-WING PITCH, COURSE ANGLE RATE, AND CLIMB RATE RESULTS UNDER WINDLESS CONDITION	12
FIGURE 14 - MULTI-ROTOR DYNAMICS SYSTEM.....	15
FIGURE 15 - MULTI-ROTOR OVERALL SYSTEM	16
FIGURE 16 - MULTI-ROTOR POSITION CONTROLLER SYSTEM	17
FIGURE 17 - MULTI-ROTOR MOTION GIVEN A RADIUS OF 10 M AND A VELOCITY OF 1 M/S.....	18
FIGURE 18 - MULTI-ROTOR SIMULATION RESULTS	18
FIGURE 19 - ABSOLUTE ERROR OF ONE FULL RATION AS A FUNCTION OF THE PATH LENGTH.....	19
FIGURE 20 - EFFECT OF INCREASING THE VELOCITY ON THE ERROR WHILST RADIUS IS CONSTANT .	19
FIGURE 21 - EFFECT OF INCREASING THE RADIUS ON THE ERROR WHILST THE VELOCITY IS CONSTANT	20
FIGURE 22- MULTI-ROTOR TOTAL POWER VS V.....	22
FIGURE 23 - MULTI-ROTOR TOTAL POWER/V VS V	22

Overview

This project focuses on the detailed design and simulation of small Unmanned Aerial Systems (UAS) for different scenarios, encompassing performance analysis and dynamics modeling. Two different configurations were explored: a fixed-wing UAV and a multi-rotor (i.e. quadrotor) drone. The project involves four key tasks for each aircraft system: performance evaluation in terms of flight range and endurance, nonlinear dynamics model derivation followed by linearization, controller design in MATLAB and Simulink, and thorough simulation analysis for various tasks.

For the fixed-wing UAV, a control system was developed to handle both desired altitude and the impact of wind on the aircraft. The aircraft underwent simulations for steady-level of flight, a 90-degree turn, an ascent, and steady-level of flight again.

The multi-rotor configuration involved the development of a position controller integrated with dynamics. The simulations were to ensure for the multi-rotor to be able to achieve desired positions in three-dimensional space.

The project emphasizes the importance of understanding the fundamental workings of unmanned aerial systems (UAS) in different configurations and their practical applications. Rigorous simulation analysis is crucial before real-world testing, and stable controller design is essential for autonomy.

The project underscores the importance of trade-offs in design, emphasizing the need to balance parameters for optimal system performance. Lessons learned include the challenge of trade-offs in PID tuning, where optimizing one parameter may impact others.

Fixed-wing

Design Objective

Given the characteristics of the fixed wing UAS, a control system was required to control the flight path of the UAS after ascending and beginning steady level flight. The control system was required to maintain steady level flight, guide the aircraft through a 90 degree turn, and ascending to a higher altitude. The control system needed the ability to take in the velocity, the radius of the turn, and the height to which to ascend too.

Aircraft Dynamics

For the aircraft dynamic model u , v , and w were defined as the ground speed in vehicle frame. These were used to develop the kinematic and dynamic models. For aerodynamic forces we calculate the airspeed $V_a = (u_a, v_a, w_a)$ by subtracting the wind speed V_w from the ground speed V_g .

Autopilot Design

The autopilot system was designed to receive high-level commands such as (h_c, V_c, R_c) where h_c is the altitude, V_c is the ground speed in body frame (forward component usually), and R_c is the turning radius. Using the equation below the turning radius was changed into turning rate $\dot{\chi}_c$, so the input reference signal for the autopilot controller was $(h_c, V_c, \dot{\chi}_c)$.

$$\dot{\chi} = \frac{V_g \cos \gamma}{R}$$

The current state of the aircraft also needed to be tracked. The state estimator covered next was used to convert the raw state of the aircraft to what the controller needed. Below is the Simulink model for the control system developed for the fixed-wing aircraft.

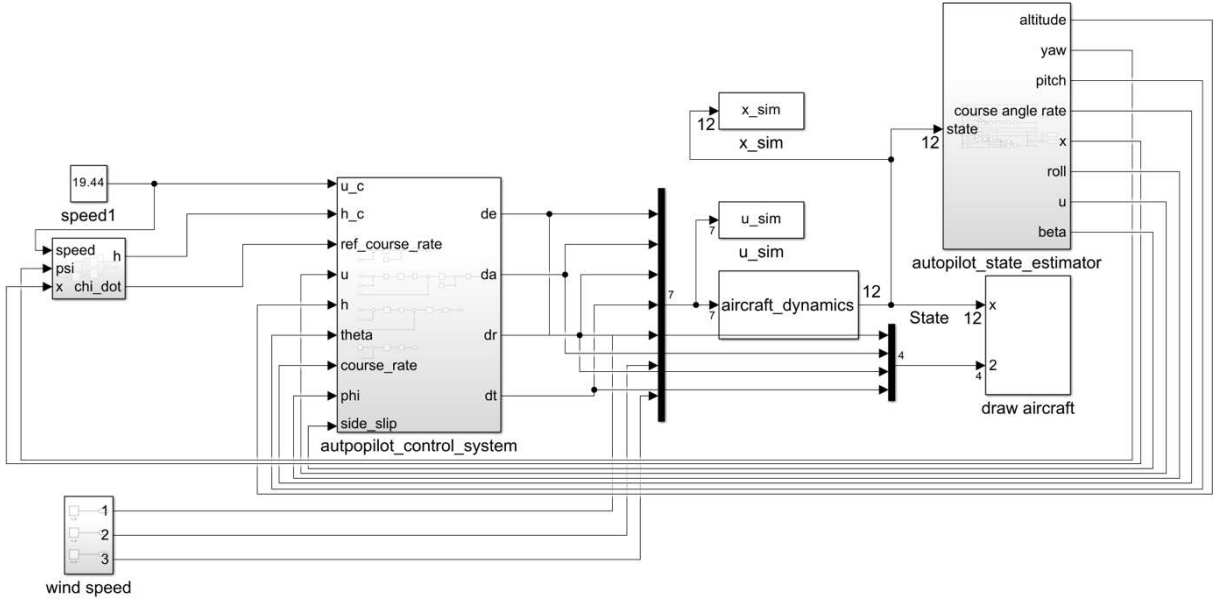


Figure 1 - Fixed-Wing overall system design

Although this project did not require a state-estimator, it still needed to convert the aircraft state into altitude h , forward speed V_g , and course angle rate $\dot{\chi}_c$ for the autopilot system. The course angle rate was approximated by the rate [1].

$$h = -p_a$$

$$V_g = u$$

$$\dot{\chi} \approx \dot{\psi} = q \sin \phi \cos \theta + r \cos \phi \cos \theta$$

Other than the states the autopilot uses, both angle of attack α , and flight path angle γ are measured as requested by the project.

$$\alpha = \tan^{-1} \left(\frac{w}{u} \right)$$

$$\gamma = \theta - \alpha$$

The state estimator block is shown below.

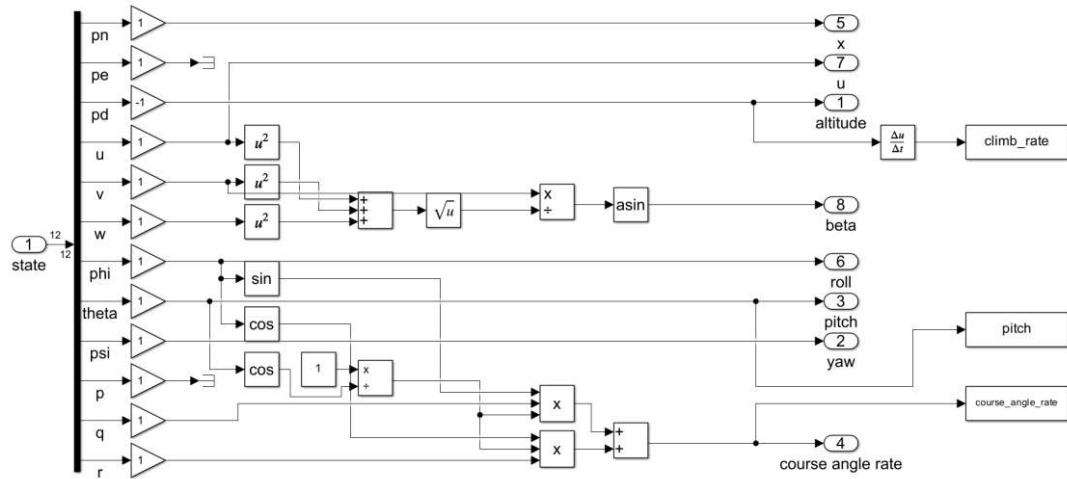


Figure 2 - Fixed-Wing state estimator system

Trim Condition

In this section the method of determining trim values used as feedforward signal in thrust and elevator are presented. These values can be helpful in reducing the gains in the PID controller (only needs to control the residual error). [1]

For thrust required for level flight, first determine initial value was determined using “Trim the model” tool in Simulink resulting in $dt_{trim} = 0.25522$. Next the controller was tuned with the initial trim value and the thrust output was measure retuning the finalized the value $dt_{trim} = 0.25$.

For elevator, the controller was directly tuned, and the elevator output was measured. The resultant was $de_{trim} = -7.3^\circ$. Following the addition of the trim condition the controller gain was retuned.

Velocity Control

The aircraft speed is controlled by varying the throttle. For the throttle the input $(0,1)$ is linearly mapped to $(0, \Omega_{max})$, where Ω_{max} is the maximum rotation speed of the propeller. The control system is shown below.

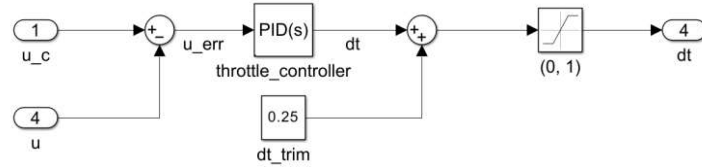


Figure 3 - Fixed-Wing control system - velocity control

The velocity controller had the following gains after tuning.

$$K_p = 1.3814 \quad K_i = 16.4 \quad K_d = 0.00372 \quad N = 244.636$$

Altitude Control

The altitude controller operates by controlling the pitch angle. The inner loop controls the elevator to return the targeted pitch angle. The middle saturation block was used to tune the rate of climb to achieve the altitude change in the given time requirement.

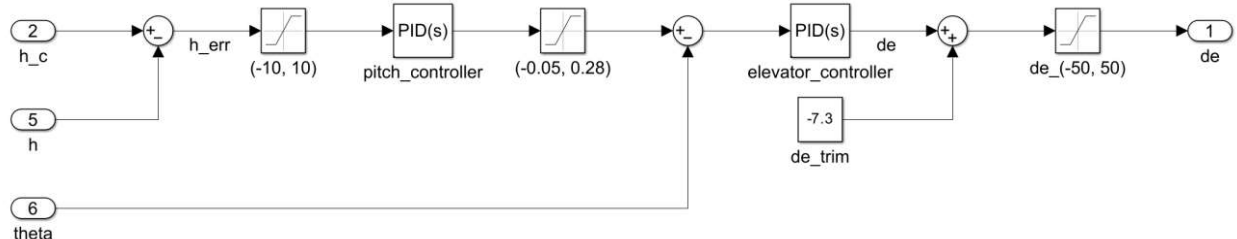


Figure 4 - Fixed-Wing control system - Altitude control

For the outer controller the gains were tuned to the following. It was found that the integral term caused instability so only a PD controller was necessary.

$$K_p = 0.3879 \quad K_i = 0 \quad K_d = 0.1105 \quad N = 33.8099$$

And the inner controller gains were tuned to the below values;

$$K_p = -227.482 \quad K_i = -182.296 \quad K_d = -64.9424 \quad N = 138.1445$$

Coordinated Turn Control

To facilitate turning, the aircraft is rolled in the turning direction using the ailerons. The inner controller controls the roll and the outer controller the ailerons.

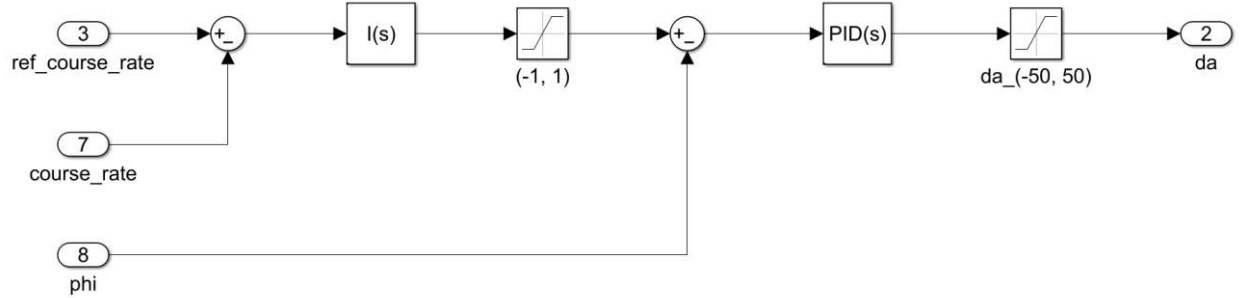


Figure 5 - Fixed-Wing control system - course rate control

After tuning, only the integral gain $K_i = 31.701$ was used for the outer loop. One hypothesis is that since the roll angle cannot be determined from the targeted course rate, it gradually rolls by accumulating the error in course angle rate.

For the inner loop, we have the following gains.

$$K_p = 100 \quad K_i = 100 \quad K_d = 15 \quad N = 81.1907$$

Sideslip Control

The sideslip is controlled using the rudder.

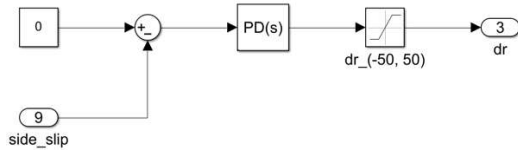


Figure 6 - Fixed-Wing control system - Sideslip control

$$K_p = 35126.8 \quad K_d = 0 \quad N = 100$$

Performance

Windless Case

The developed controller was implemented to perform the simulation model in Simulink. The plots below were obtained and indicate our fixed-wing model maintains a steady level of flight for 250 m at $70 \frac{\text{km}}{\text{h}}$, which is at 19.44 m/s. Subsequently, the fixed-wing model demonstrates its maneuverability by executing a 90° turn with a radius of 250 m. Following this maneuver, the fixed-wing successfully accomplishes an ascent from 1,000 m to 1,100 m in 29 s, meeting the specified requirement. Upon completion of the ascent, the fixed-wing model returns to a steady level of flight and maintains the altitude, showing the robustness and adaptability of the developed control system. The simulation results underscore the effectiveness of our flight control system in handling windless conditions and meeting the designated performance criteria.

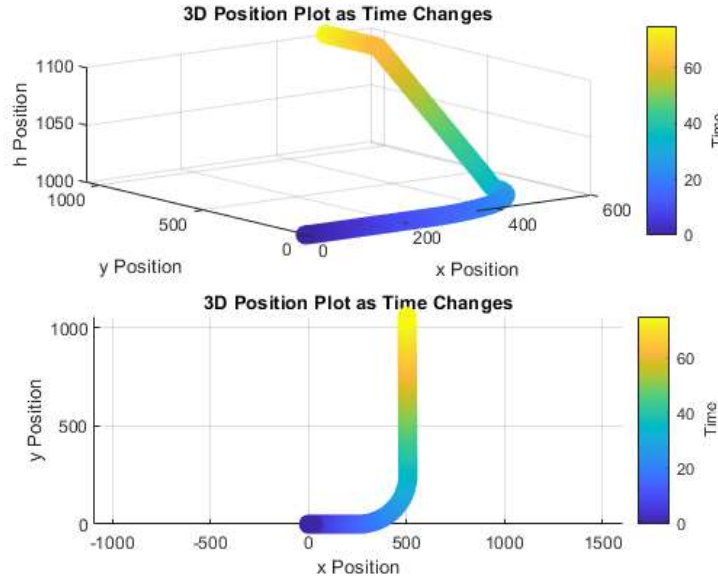


Figure 7 - Fixed-Wing 3D Position Plot as Time Changes under windless condition - 3D view (top) & x-y view (bottom)

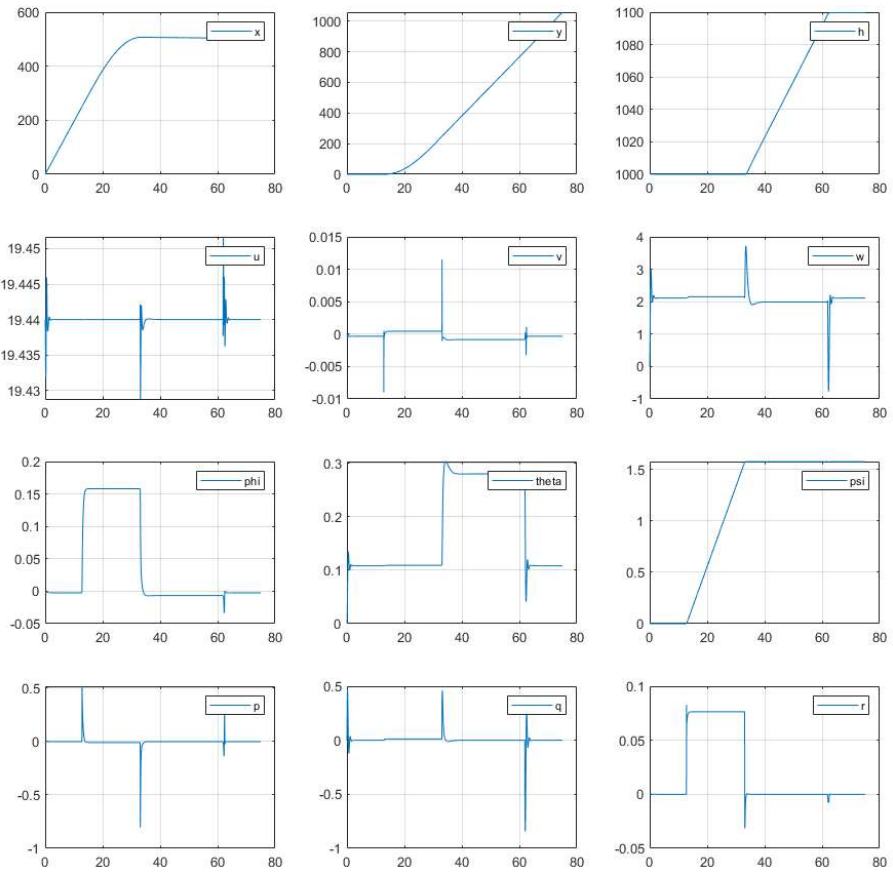


Figure 8 - Fixed-Wing simulation results under windless condition

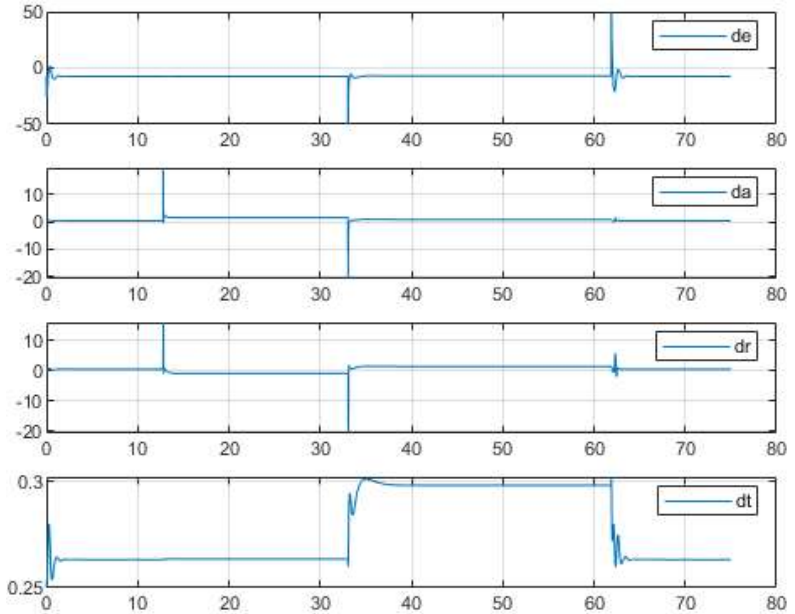


Figure 9 - Fixed-Wing de , da , dr , and dt results under windless condition

Wind Case

Wind components in u , v , and w were developed to control environmental conditions and determine the recommended maximum wind speed for safe operations. A trial and error method was used to identify the optimized values for the wind components. To maintain the system under control, the following values were found through the optimization: $u = 2.80$, $v = 4.10$, $w = 8.30$; however, w was disregarded for real-world relevance. Consequently, only u and v were considered in calculating the maximum wind speed, determined to be 4.96 m/s , which is 9.64 knot . This comprehensive approach ensures that the system remains under control while factoring in practical considerations. The calculated maximum wind speed serves as a valuable metric for guaranteeing safe operations in varying wind conditions.

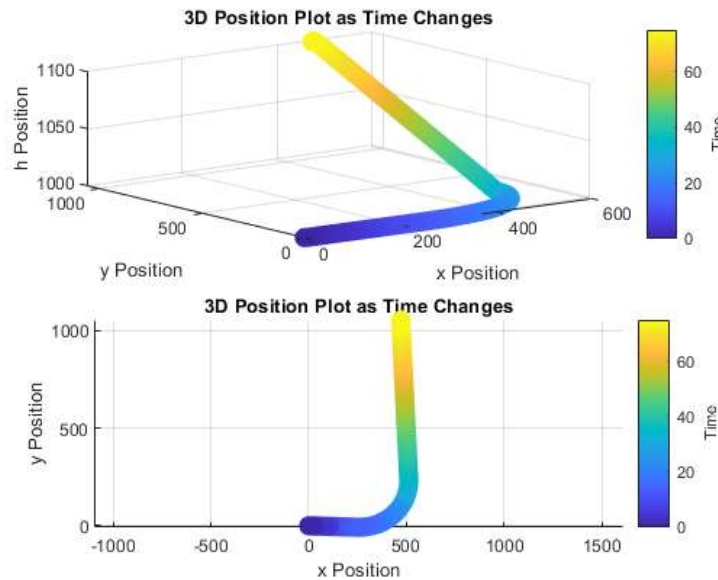


Figure 10 - Fixed-Wing 3D Position Plot as Time Changes under wind condition - 3D view (top) & x-y view (bottom)

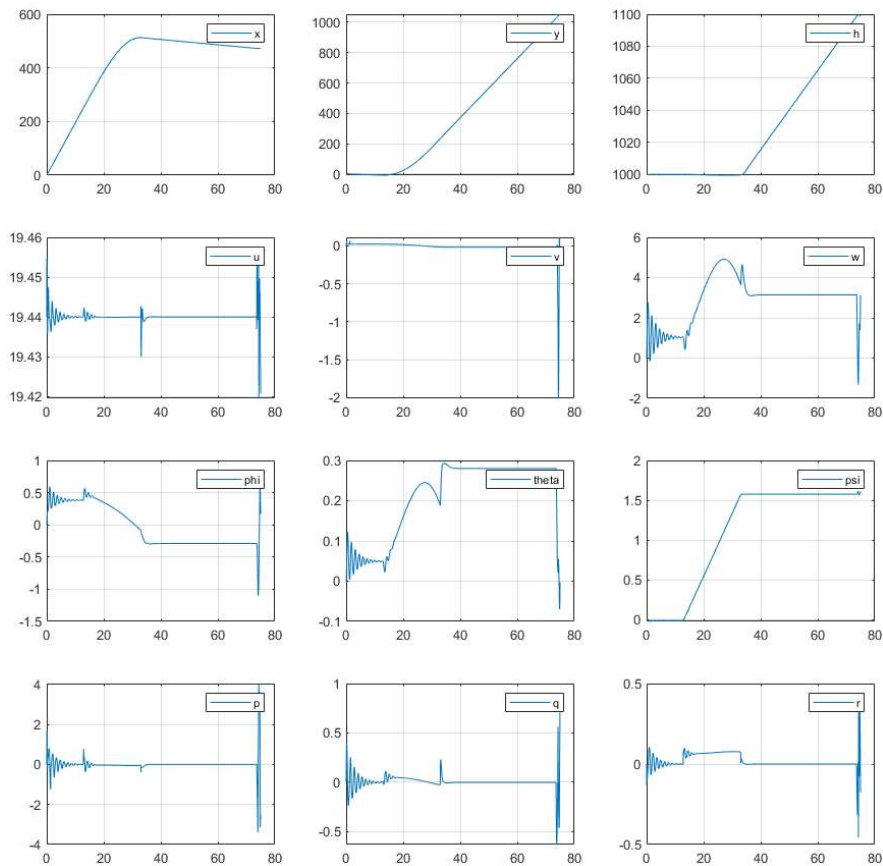


Figure 11 - Fixed-Wing simulation results under wind condition

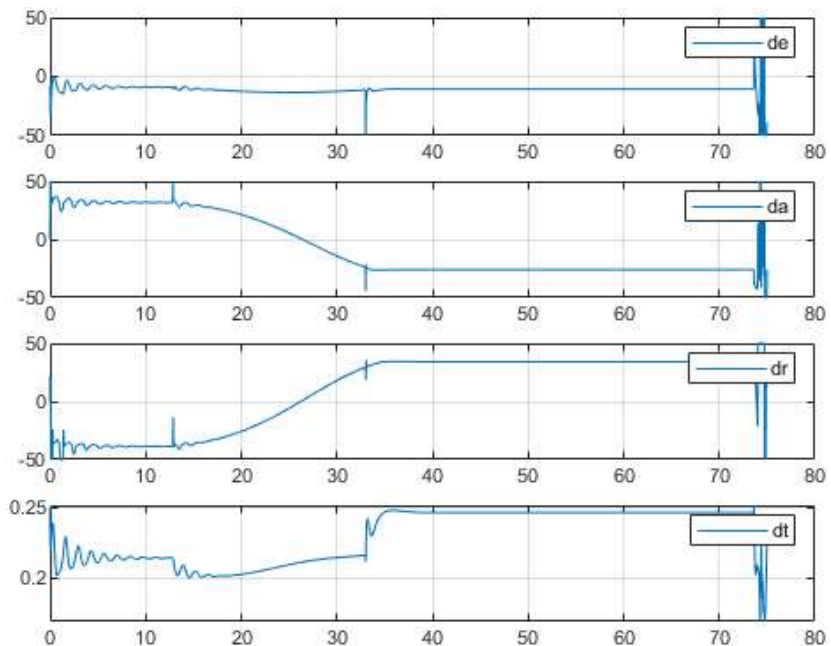


Figure 12 - Fixed-Wing de , da , dr , and dt results under wind condition

Theoretical Result vs Simulation

Angle of Attack

For steady level flight $F_L = W = mg$. The lift force at steady level flight can be calculated as,

$$F_L = \frac{1}{2} \rho V_a^2 (C_{L_0} + C_{L_\alpha} \alpha)$$

Rearranging the above equation for angle of attack results in,

$$\alpha = \frac{1}{C_{L_\alpha}} \left(\frac{2F_L}{\rho V_a^2} - C_{L_0} \right)$$

Having been given all the variables in the above equation the theoretical angle of attack was evaluated to be 0.08 radians, or 4.57° .

The simulation results in Figure 13 show the angle of attack, yaw rate, and climb rate in different phases of the operation. During steady level flight, since flight path angle is 0, angle of attack is the same as pitch angle at 0.11 radian. Such differences can be due to nonzero input to elevator to maintain pitch angle.

Yaw Rate

For the coordinated turn the yaw rate can be calculated using the equation below.

$$\dot{\chi} = \frac{V_g \cos \gamma}{R}$$

Evaluating the above equation with the givens results in a yaw rate of 0.078 rad/s .

During coordinated turn without wind, the yaw rate is the same as the course angle rate. From the results in Figure 13 the simulation course angle can be observed to be 0.08 rad/s which matches our expectation.

Climb Rate

The pitch angle θ has a saturation limit of 0.28 radians, therefore the max climb rate is limited by the flight path angle. The flight path angle can be evaluated to be 0.2 radians using the equation below.

$$\gamma_{max} = \theta - \alpha$$

Using the flight path angle the rate of climb can be evaluated using the equation below and results in a 3.94 m/s

$$(R/C)_{max} = V \sin \gamma = u \tan \gamma$$

Finally, during steady climbing, the aircraft maintains a max flight path angle of 0.28 radian during the climb, thus the max climb rate matches the expectation. The entire climbing to the indented altitude takes approximately 29 seconds, thus the average climb rate is $3.43 \frac{m}{s}$ which is not far from the estimate give that it takes time to begin climbing and level out.

The table below summarizes the results from this section.

Table 1 - Summary of simulation vs theoretical results

	Angle of Attack [rad]	Yaw Rate [rad/s]	Climb Rate [m/s]
Calculation	0.08 rad	0.077 rad/s	3.94 m/s
Simulation	0.11 rad	0.08 rad/s	3.43 m/s

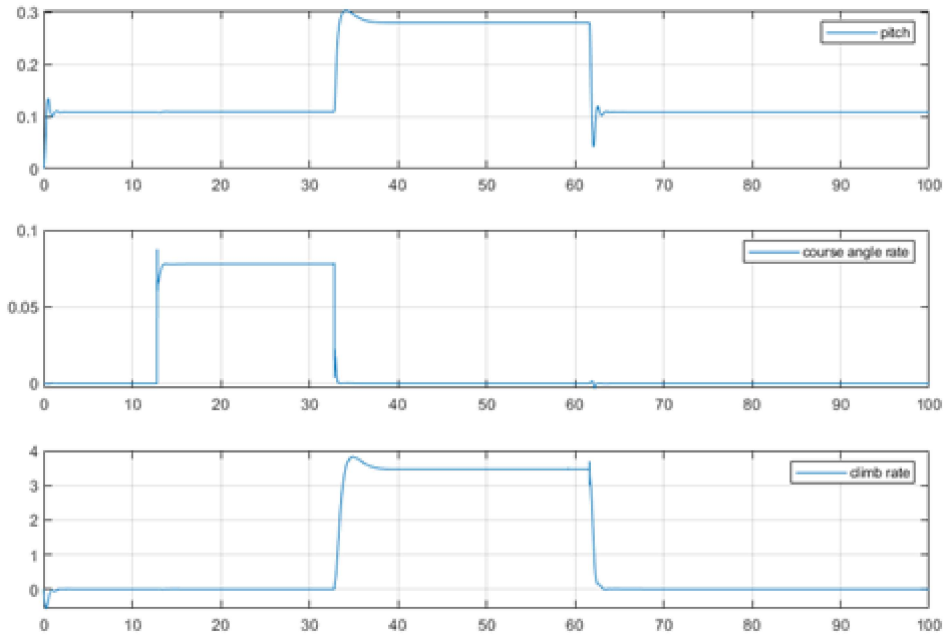


Figure 13 - Fixed-Wing pitch, course angle rate, and climb rate results under windless condition

Range and Endurance Calculations

For estimating the range and endurance, since in the project the aircraft operates mostly at an altitude of 1 km, we will use the air density at this altitude which is approximately $1.1116 \frac{kg}{m^3}$.

Endurance

For estimating endurance the aircraft is assumed to be operating at the minimum power required to maintain level flight. The lift coefficient in the minimum power condition was evaluated to be 1.14 using the equation below.

$$C_L^* = \sqrt{\frac{C_{D_0}}{K}} = \sqrt{C_{D_0} \pi e \left(\frac{b}{c}\right)}$$

From the SPC definition the following equation can be derived,

$$c_p = \frac{\eta}{P} \frac{dW}{dt} \Rightarrow dt = \frac{1}{c_p P} dW$$

Since power $P = TV$, integrating the equation above results in the endurance equation below.

$$E = \frac{\eta}{c_p} \sqrt{2\rho S} \frac{(C_L)^{3/2}}{C_D} \left(\frac{1}{\sqrt{W_1}} - \frac{1}{\sqrt{W_0}} \right)$$

Since the only non-constant variables are C_L and C_D , then to maximise the endurance the aircraft must operate in a condition that maximises $\frac{C_L^{3/2}}{C_D}$.

$$\frac{C_L^{3/2}}{C_D}_{max} = \frac{1}{4C_{D_0}} \left(\frac{3C_{D_0}}{K} \right)^{\frac{3}{4}}$$

Evaluating the endurance with all the given variables results in 55 hours.

Range

To evaluate the range, the distance traveled is integrated from the initial weight to the final weight with respect to the time it took. The equations below show how this can be evaluated.

$$R = \int_{W_0}^{W_1} V dt = \int_{W_0}^{W_1} \frac{\eta}{SPC} \frac{V}{P} dW = \int_{W_0}^{W_1} \frac{\eta}{SPC} \frac{1}{T} dW$$

Since at level flight $T = D$ where $D = 0.5 \rho S V^2 C_D$ and $V = \sqrt{\frac{2W}{\rho S C_L}}$, the above equation can be simplified to the following,

$$R = \int_{W_0}^{W_1} \frac{\eta}{SPC} \frac{2}{\rho S V^2 C_D} dW = \int_{W_0}^{W_1} \frac{\eta}{SPC} \frac{C_L}{C_D} \frac{dW}{W}$$

Integrating the equation results in the range equation used.

$$R = \frac{\eta}{c_p} \frac{C_L}{C_D} \ln \left(\frac{W_0}{W_1} \right)$$

Similar to the endurance the only non-constant values are the C_L and C_D . To maximise range the C_L/C_D ratio must be maximised which can be achieved using $C_L/C_D = 1/\sqrt{2KC_{D_0}}$. Evaluating the range equation with all the known variables results in a range of 3048 km.

Multi-Rotor

Design Objective

A control system was required to navigate a multi-rotor system to hover at a fixed point, then transition into a circular motion given the velocity, central position, and radius. For the initial analysis of the simulation the hovering point was designated as $(x, y, z) = (0, 0, 2)$, and the center of the circular motion was $(x, y, z) = (0, 0, -3)$. A series of velocity and radii were evaluated using the designated center position to evaluate the robustness of the control system. The performance of the control system was measured using the mean error of one full rotation about the circular path.

Multi-rotor Dynamics

For the multi-rotor dynamics, the closed-loop angle control for roll, pitch, and yaw were provided as separate state space models. Additionally, the state space models for vertical speed to height, pitch to u , and roll to v were provided. The figure below shows the block diagram of the dynamics.

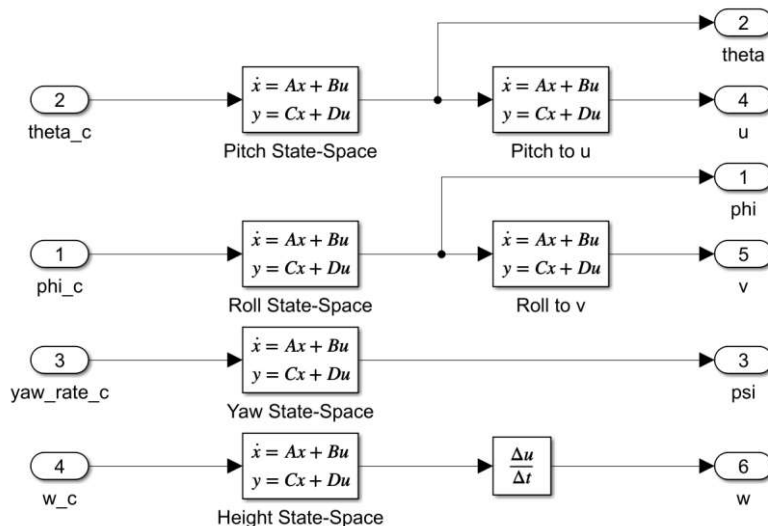


Figure 14 - Multi-Rotor dynamics system

The table below summarizes the inputs and outputs of each of the dynamics systems.

Table 2 - State-Space Inputs and Outputs Used For Dynamics Model

Name	Input	Output
Roll	Desired roll angle	Actual roll angle
Pitch	Desired pitch angle	Actual pitch angle
Yaw Rate	Desired yaw rate in rad/s	Actual yaw angle in rad
Height	Vertical speed	Actual height
Pitch to u	Actual pitch angle	Actual forward velocity in body frame (u)
Roll to v	Actual roll angle	Actual sideways velocity in body frame (v)

Control Design

Since the control system needed to work for both hover (position tracking) and orbiting at fixed velocity and radius (trajectory tracking), the controller was designed with $(x_0, y_0, z_0, \omega, R)$ as inputs where (x_0, y_0, z_0) is the center of the circular trajectory. If $R = 0$ the tracking problem falls back to fixpoint tracking. Below is our overall system design.

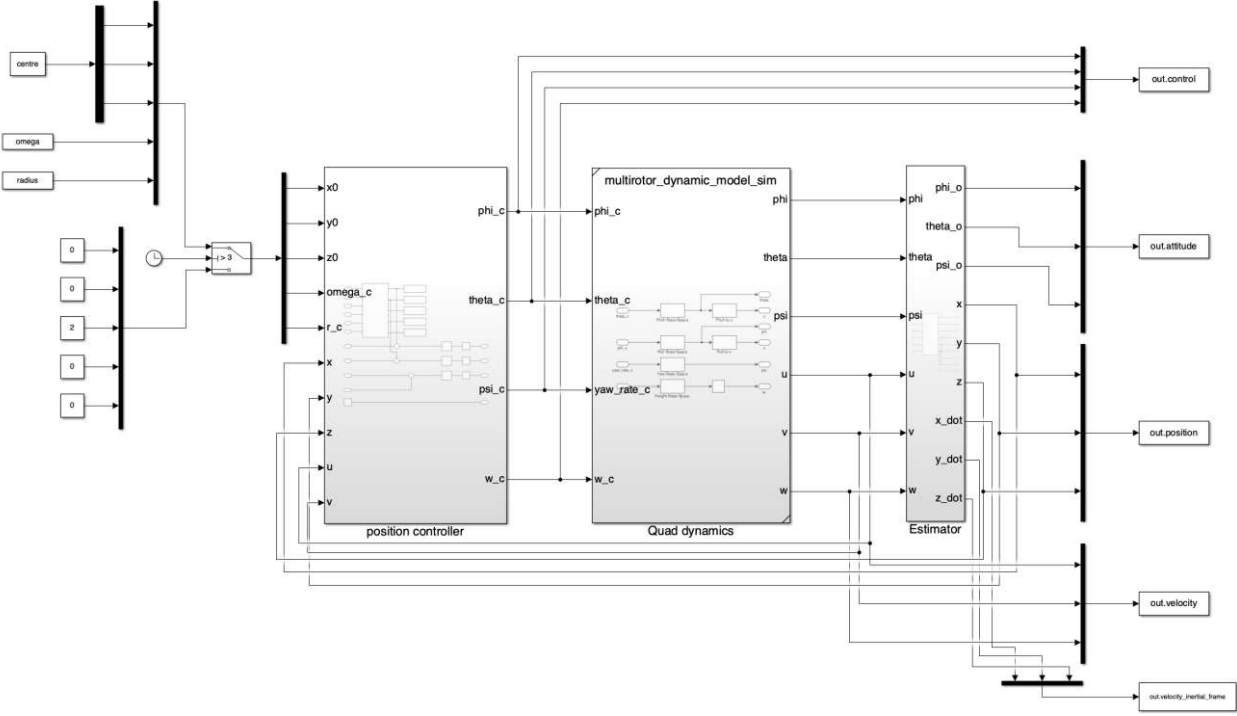


Figure 15 - Multi-Rotor overall system

The aim of the controller design was to decouple each axis (roll, pitch, yaw, and height) such that tuning can be done independently. For additional simplification the yaw angle was fixed by tracking $\psi = 0$. The control in the z axis is done through the vertical speed w .

To achieve both fixpoint tracking and trajectory tracking, a reference calculation function was used to calculate the decomposed reference velocity (u_c, v_c) given the controller input $(x_0, y_0, z_0, \omega, R)$ and current planar position (x, y) . Effectively the reference velocity is a combination of cross track error and targeted orbiting velocity.

$$V = \omega R$$

$$\gamma = \tan^{-1} \left(\frac{y - y_0}{x - x_0} \right)$$

$$e_x = x_0 + R \cos \gamma - x$$

$$e_y = y_0 + R \sin \gamma - y$$

$$u_c = V \cos(\gamma + 0.5\pi) + e_x$$

$$v_c = V \sin(\gamma + 0.5\pi) + e_y$$

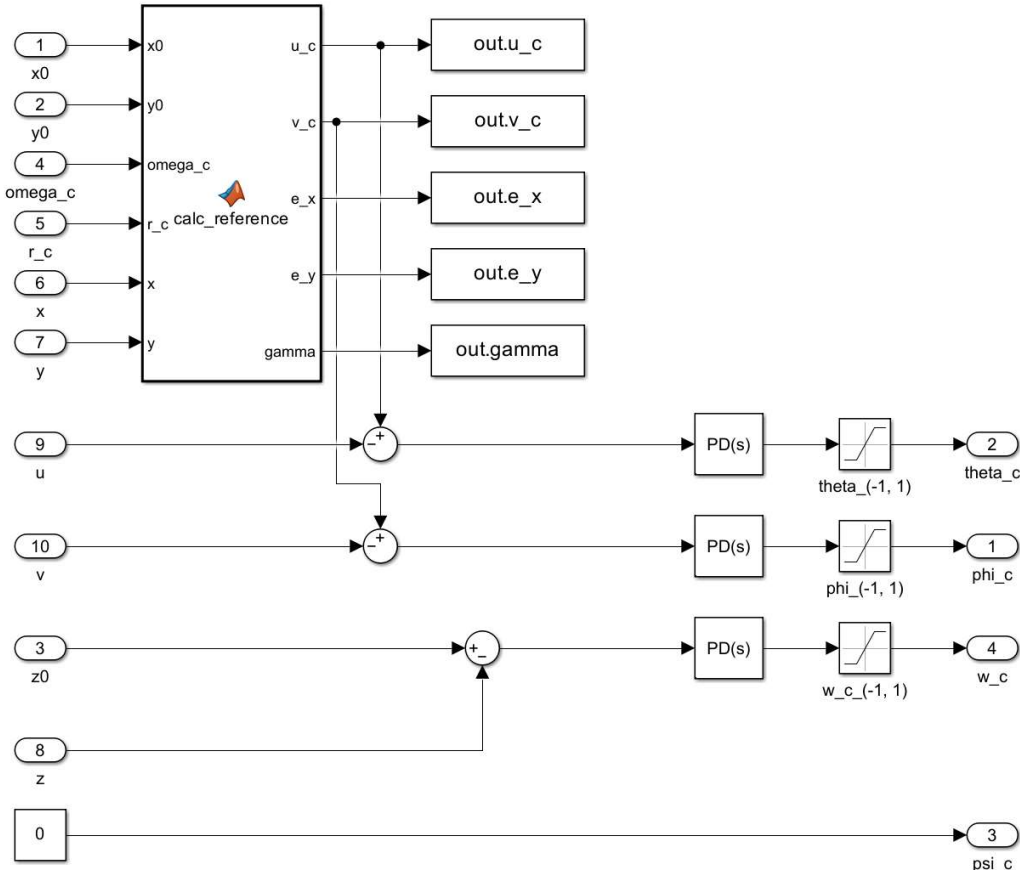


Figure 16 - Multi-rotor position controller system

For the controllers shown in the figure above only PD controllers were used as integral terms were led to instability in the response. Below are the tuned gain values for the system shown above.

$$\theta: K_p = -2.3494 \quad K_d = -3.9257 \quad N = 94.7706$$

$$\phi: K_p = 2.9409 \quad K_d = 3.9131 \quad N = 147.7696$$

$$\dot{z}: K_p = 64.94 \quad K_d = 2 \quad N = 28.4037$$

Performance

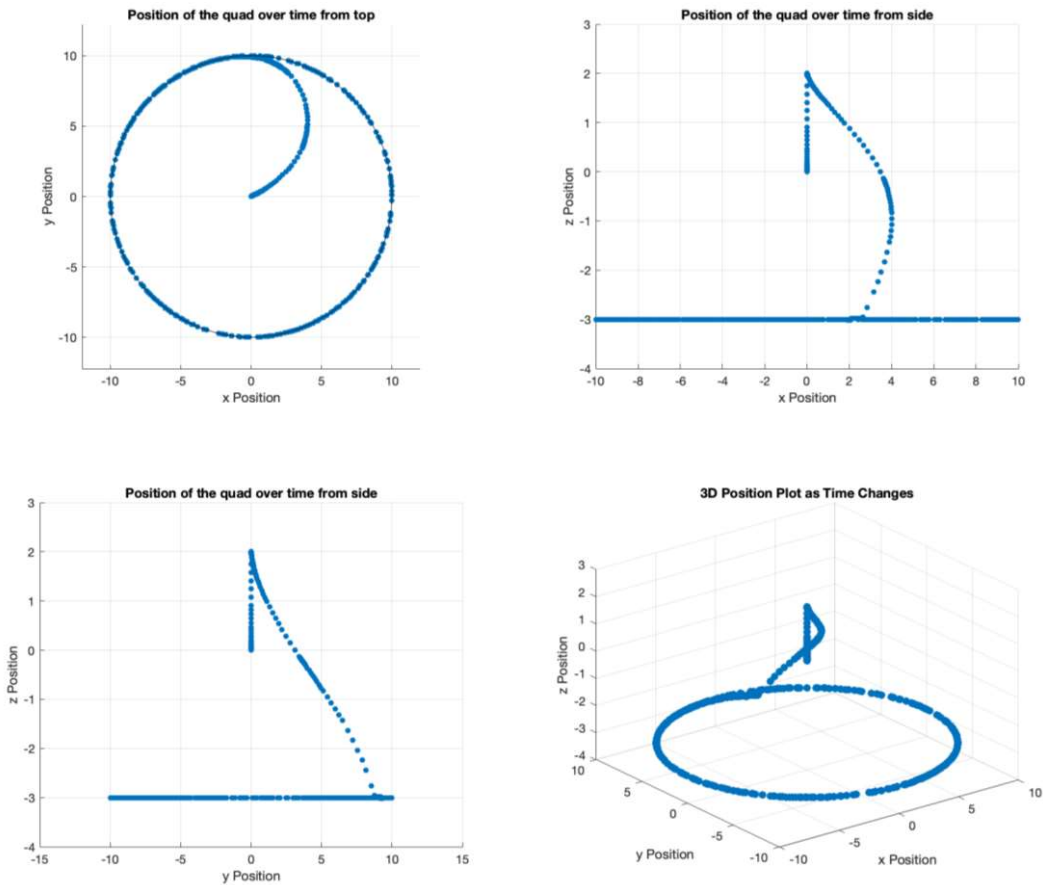


Figure 17 - Multi-rotor motion given a radius of 10 m and a velocity of 1 m/s

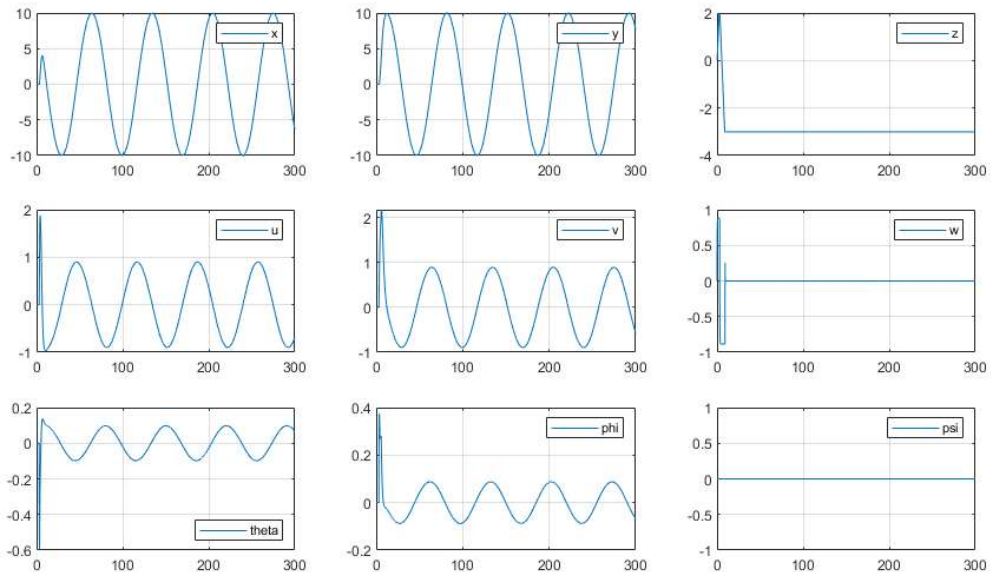


Figure 18 - Multi-rotor simulation results

From the plots shown above it can be noted that the multi-rotor drone performs the desired tasks. It climbs to the first position, $(x, y, z) = (0, 0, 2)$, then descends to the circular motion about the centre point, $(x, y, z) = (0, 0, -3)$ with a radius of 10 m. This performance of the control system was measured using the mean error of one full rotation about the circular path. The figure below shows the absolute error of between the intended position of the multi-rotor and the actual position for one full rotation of the craft. The x-axis is a fraction of the length along the full rotation. To quantify this error the mean value of this data was used, which for $R = 10$ m and $v = 1$ m/s is 0.0032 m.

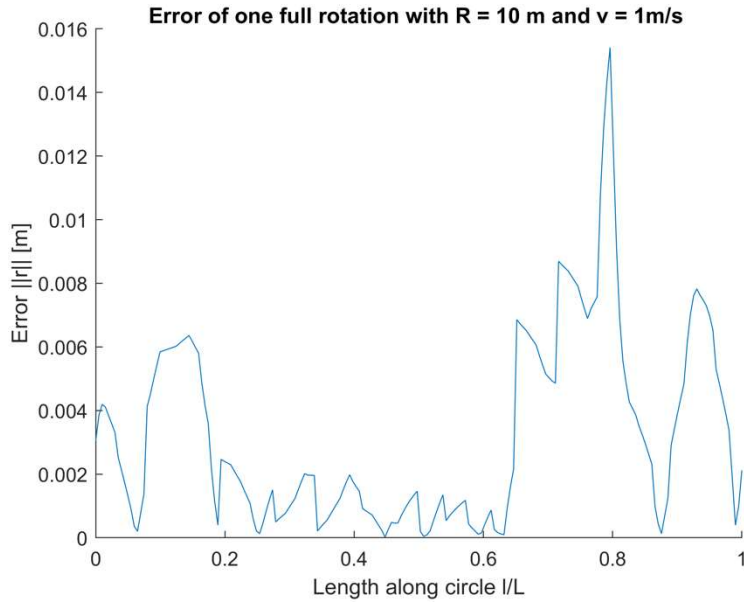


Figure 19 - Absolute error of one full ration as a function of the path length

Additional radii and velocities were also evaluated to further evaluate the accuracy of the system.

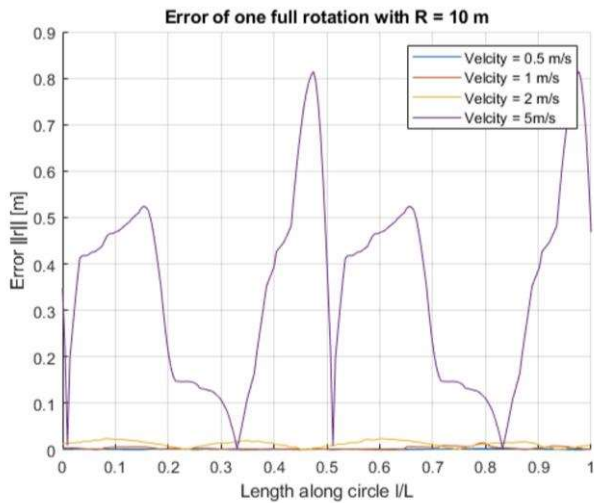


Figure 20A - Error along the length of one rotation

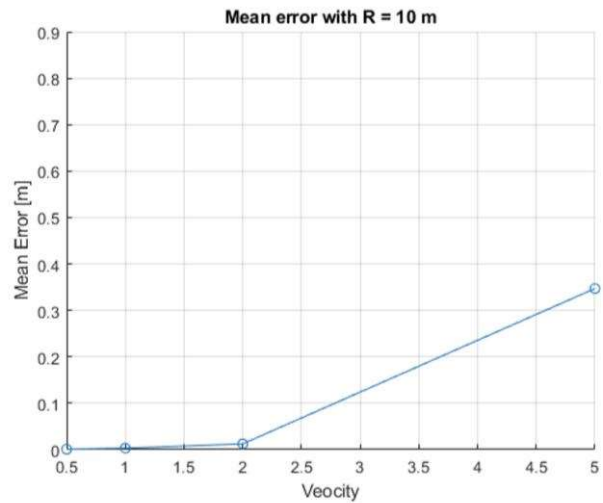


Figure 20B - Mean error of one rotation

Figure 20 - Effect of increasing the velocity on the error whilst radius is constant

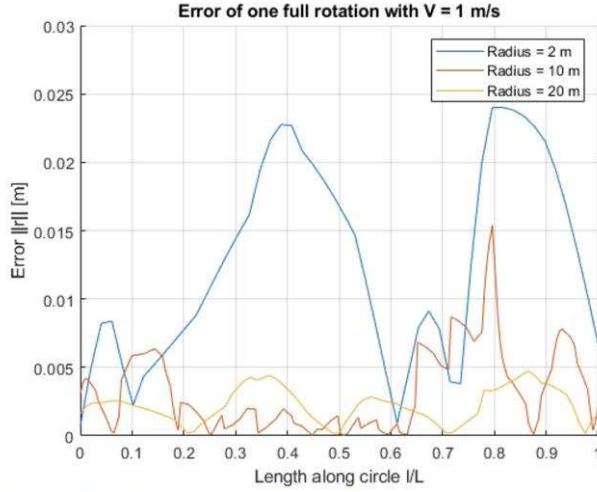


Figure 21A - Error along the length of one rotation

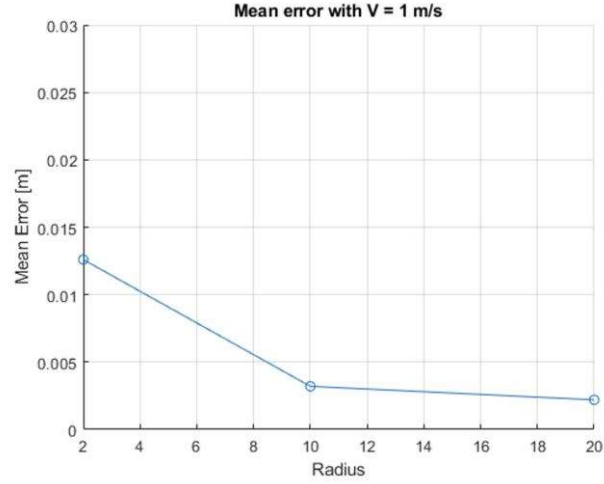


Figure 21B - Mean error of one rotation

Figure 21 - Effect of increasing the radius on the error whilst the velocity is constant

Figure 20 and Figure 21 both contain two plots. The left plot shows the magnitude of error through the length of one full rotation, for different cases of velocity and radii in Figure 20 and Figure 21 respectively. The right plots show the mean error of each of the cases presented in the respective right plot. From these it becomes clear that the error of the will increase when the radius is decreased, or the velocity is increased. This may suggest that the error is proportional to the angular velocity, but this is not the case. This can be seen if the two case with $R = 10 \text{ m}$ and $V = 5 \text{ m/s}$ and $R = 2 \text{ m}$ and $V = 1 \text{ m/s}$ are compared. Both cases have a angular velocity of 0.5 rad/s but they in fact do not have matching errors. It can therefore be concluded that the error is in fact a function of the forward velocity and radius as well, and not just to angular velocity.

The effect of each of the PD controller gains on the error is shown below to provide further insight. To evaluate these a stable model was the starting point and gains were multiplied by factors of 2 in sequence. As shown the gains from the u and v have similar behaviors for both the proportional and derivative gains. Of note is the behavior of the derivative term in the bottom plot which is the z position control. This term behaves very similarly to the proportion terms of the previous two plots. Given that all three of these terms relate to the velocity an individual direction causes this similarity.

Range and Endurance

Given the multi-rotor is not designed to operate at high altitudes the sea-level air density was used for calculating the range and endurance. $\rho = 1.225 \text{ kg/m}^3$. Additionally, using 0th order battery model we have $E = 3 \times 3.7 \times 1.5 \times 3600 = 59940 \text{ J}$. To evaluate the range and endurance forward flight momentum theory and 0th order battery model was assumed. The system has an efficiency of 70% and 80% for the motor and ESC respectively. From forward flight momentum theory we have,

$$v = \frac{T}{2\rho A \sqrt{V^2 \cos^2 \alpha_D + (v + V \sin \alpha_D)^2}}$$

To solve the above equation the solution for α_D , v , T , P_{ind} , and P_{tot} was acquired. Given the frame drag $D_f = \frac{1}{2}\rho C_d SV^2$ at $\alpha_D = 0$, and $T = \sqrt{W^2 + D_f^2}$ we can solve for $\alpha_D = \tan^{-1}(D/W)$ resulting in the equation below.

$$v^2 = \frac{T^2}{4\rho^2 A^2 (V^2 \cos^2 \alpha_D + (v + V \sin \alpha_D)^2)}$$

This equation can be also expressed as,

$$v^4 + (2V \sin \alpha_d)v^3 + v^2 V^2 - \frac{(W^2 + D^2)}{4\rho^2 A^2} = 0$$

Given the above is in a quartic expression, solving for the real root will give the result for v . Solving for v allows for the total power used to be solved.

$$P_{tot} = T(v + V \sin(\alpha_D))$$

The plots below were generated by varying the velocity from 0 to 20 m/s. The plot on the left shows the total power over this range, and the plot on the right is the total power divided by the velocity. The maximum endurance occurs when the plot on the left is at its minimum, and maximum range occurs when the plot on the right is at its minimum. Both points are identified with a red circle on the plots.

The total power from these points was used in the equation below to find the flight time. This resulted in the maximum endurance, and the maximum range was evaluated by multiplying the time by the respective flight speed.

$$t = \frac{E_b \eta_m \eta_e}{P_{tot}}$$

The maximum endurance was 60 minutes with a forward speed of 7.0 m/s.

The maximum range was 29.92 km with a forward velocity of 9.5 m/s.

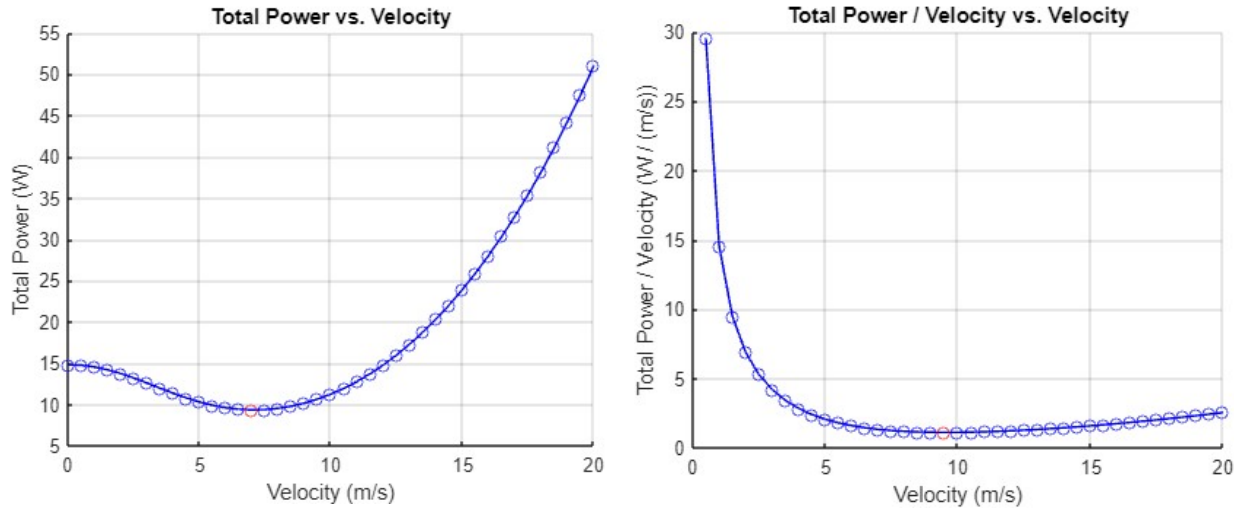


Figure 22- Multi-Rotor Total Power vs V

Figure 23 - Multi-Rotor Total Power/ V vs V

Conclusions and Lessons Learned

The technical conclusions drawn from the implementation of fixed-wing and multi-rotor Unmanned Aerial System (UAS) configurations include several key observations:

1. Theoretical values derived from theories like Forward Flight Momentum Theory or 0^{th} order battery model may significantly differ from actual flying system values due to assumptions and data inconsistencies.
2. Implementing non-linear dynamics provides more accurate simulations compared to a linearized system, although linearization is beneficial for understanding system properties.
3. Unrealistic range and endurance values in both fixed-wing and multirotor aircraft are attributed to data inconsistencies.
4. Saturation can help the system with both large and small errors.

The project served as a learning opportunity for developing an Autopilot system, with significant lessons in working with MATLAB and Simulink, setting up control blocks, and designing control systems. The experience provided a strong foundation in control system design and development.

In conclusion, MATLAB and Simulink simulations and modeling were conducted on fixed-wing UAV and quad-rotor drone configurations. Range and endurance estimates were calculated, and control algorithms were developed and tested for both configurations. Notable lessons include the impact of controller optimization on trade-offs, interpreting simulation results' physical significance, sensitivity to trim correctness, and the advantages and challenges of non-linear and linear dynamics models.

The primary project focus was on developing control designs for autonomous flight in unmanned aerial systems. Flight stability was found to depend significantly on trim calculation correctness, and revisions improved stability. Key lessons emphasized the importance of interpreting simulation results, sensitivity to trim correctness, and the trade-offs between non-linear and linear dynamics models. Additionally, having effective visualization tools was crucial for interpreting simulation results at various stages.

The main work was divided into nine main parts, with three individual components.

1. Range & Endurance Calculations (Fixed-Wing): _____ Victor Gao
2. Range & Endurance Calculations (Multi-Rotor): _____ Min Woo Kong
3. Fixed Wing Control System Development: _____ Victor Gao and Min Woo Kong
4. Fixed Wing Control System Tuning and Simulation: _____ Everyone
5. Multirotor Control System Development: _____ Victor Gao and Pouya Asgharzadeh
6. Multirotor Control System Tuning and Simulation: _____ Victor Gao and Pouya Asgharzadeh
7. Setting up the System for Final Simulation & all Maneuvers: _____ Everyone
8. Documentation & Presentation: _____ Everyone
9. Report formatting and proofing: _____ Pouya Asgharzadeh

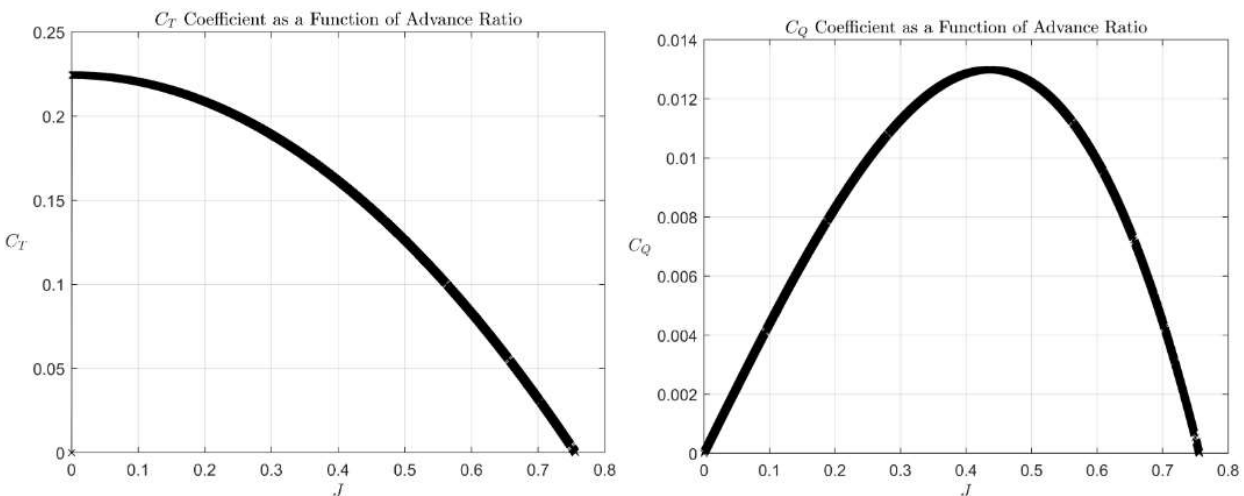
Though we needed to divide the work, working together on the simulation and documentation provided each one of us with thorough knowledge of both the Fixed-Wing and Multi-rotor control systems.

References

- [1] Randal W Beard and Timothy W McLain. Small unmanned aircraft. Princeton university press, 2023.
- [2] UIUC. Propeller Data. URL: <https://m-selig.ae.illinois.edu/props/volume-1/propDB-volume-1.html#APC>

Appendix A: Fixed-wing Data

Geometric Data		Longitudinal		Lateral	
Parameter	Value	Coef.	Value	Coef.	Value
m	9.1 kg (Empty)	C_{L_0}	0.28	C_{Y_0}	0
I_{xx}	0.8244 kg m ²	C_{D_0}	0.03	C_{l_0}	0
I_{yy}	1.135 kg m ²	C_{m_0}	-0.02338	C_{n_0}	0
I_{zz}	1.759 kg m ²	C_{L_α}	3.45	C_{Y_β}	-0.98
I_{xz}	0.1204 kg m ²	C_{D_α}	0.30	C_{l_β}	-0.12
S	0.55 m ²	C_{m_α}	-0.38	C_{n_β}	0.25
b	2.8956 m	C_{L_q}	0	C_{Y_p}	0
c	0.18994 m	C_{D_q}	0	C_{l_p}	-0.26
S_{prop}	0.2027 m ²	C_{m_q}	-3.6	C_{n_p}	0.022
e	0.9	$C_{L_{\delta_e}}$	-0.36	C_{Y_r}	0
C_T	See below	$C_{D_{\delta_e}}$	0	C_{l_r}	0.14
C_Q	See below	$C_{m_{\delta_e}}$	-0.5	C_{n_r}	-0.35
Ω_{max}	12500 RPM			$C_{Y_{\delta_a}}$	0
Fuel Capacity	4.0 kg			$C_{l_{\delta_a}}$	0.08
SFC	0.6651 g/hr/W			$C_{n_{\delta_a}}$	0.06
				$C_{Y_{\delta_r}}$	-0.17
				$C_{l_{\delta_r}}$	0.105
				$C_{n_{\delta_r}}$	-0.032



Appendix B: Multi-Rotor State Space Model

- Roll: The input for roll is desired roll angle (rad), and the output is actual roll angle (rad).

$$A = \begin{bmatrix} -4.2683 & -3.1716 \\ 4 & 0 \end{bmatrix} \quad B = \begin{bmatrix} 2 \\ 0 \end{bmatrix}$$

$$C = [0.7417 \ 0.4405] \quad D = [0]$$

- Pitch: The input for pitch is desired pitch angle (rad), and the output is actual pitch angle (rad).

$$A = \begin{bmatrix} -3.9784 & -2.9796 \\ 4 & 0 \end{bmatrix} \quad B = \begin{bmatrix} 2 \\ 0 \end{bmatrix}$$

$$C = [1.2569 \ 0.6083] \quad D = [0]$$

- Yaw: The input for yaw is desired yaw rate (rad/s), and the output is actual yaw angle (rad).

$$A = [-0.0059] \quad B = [1]$$

$$C = [1.2653] \quad D = [0]$$

- Height: The input for height is desired vertical speed (m/s), and the output is actual height (m).

$$A = \begin{bmatrix} -5.8200 & -3.6046e^{-6} \\ 3.8147e^{-6} & 0 \end{bmatrix} \quad B = \begin{bmatrix} 1024 \\ 0 \end{bmatrix}$$

$$C = [1.4907e^{-4} \ 1.3191e^3] \quad D = [0]$$

- Pitch to u: The input for the pitch to u is the actual pitch angle (rad), and the output is actual forward velocity u (m/s).

$$A = [-0.665] \quad B = [2]$$

$$C = [-3.0772] \quad D = [0]$$

- Roll to v: The input for the roll to v is the actual roll angle (rad), and the output is actual sideway velocity v (m/s).

$$A = [-0.4596] \quad B = [2]$$

$$C = [2.3868] \quad D = [0]$$